

Realtime automatic metal extraction of medical x-ray images for contrast improvement

Martin Prangl^a, Hermann Hellwagner^a, Christian Spielvogel^a, Horst Bischof^b
and Tibor Szkaliczki^c

^aDepartment of Information Technology, Klagenfurt University, Universitätsstr. 65 - 67,
9200 Klagenfurt, Austria;

^bDepartment of Computer Vision and Graphics, Technical University Graz, Inffeldgasse 16/II,
8010 Graz, Austria;

^cDepartment of eLearning, Computer and Automation Research Institute of the Hungarian
Academy of Sciences, 1111 Budapest XI. Lagymányosi u. 11, Hungary

ABSTRACT

This paper focuses on an approach for real-time metal extraction of x-ray images taken from modern x-ray machines like C-arms. Such machines are used for vessel diagnostics, surgical interventions, as well as cardiology, neurology and orthopedic examinations. They are very fast in taking images from different angles. For this reason, manual adjustment of contrast is infeasible and automatic adjustment algorithms have been applied to try to select the optimal radiation dose for contrast adjustment. Problems occur when metallic objects, e.g., a prosthesis or a screw, are in the absorption area of interest. In this case, the automatic adjustment mostly fails because the dark, metallic objects lead the algorithm to overdose the x-ray tube. This outshining effect results in overexposed images and bad contrast. To overcome this limitation, metallic objects have to be detected and extracted from images that are taken as input for the adjustment algorithm. In this paper, we present a real-time solution for extracting metallic objects of x-ray images. We will explore the characteristic features of metallic objects in x-ray images and their distinction from bone fragments which form the basis to find a successful way for object segmentation and classification. Subsequently, we will present our edge based real-time approach for successful and fast automatic segmentation and classification of metallic objects. Finally, experimental results on the effectiveness and performance of our approach based on a vast amount of input image data sets will be presented.

Keywords: Pattern recognition, Segmentation, Medical imaging, X-Ray, Artefact-Segmentation

1. INTRODUCTION

Medical imaging becomes more and more important. Modern techniques are able to assist in medical treatment and diagnostic decisions. In this paper, we focus on a contrast improvement solution for medical digital x-ray systems, so called C-arms. C-arms are x-ray systems which are able to take images from different angles of the region of interest (ROI) and are used for vessel diagnostics, surgical interventions, and for cardiology, neurology and orthopedic examinations. Modern C-arms are very fast, they are able to take about 30 digital images per second and they will get faster in the future. This makes it possible to control surgeries online.¹ Because image series are taken fast from different angles, manual adjustment of contrast is impractical. Therefore, automatic histogram based algorithms are used to adjust the dose of the x-ray tube and consequently the contrast. Two images are taken during this process. The first image is taken by a standard dose. Its grayscale distribution is analyzed and an appropriate dose for the second image is calculated. Problems occur in these adjustment

Further author information: (Send correspondence to M.P.)

M.P.: E-mail: martin.prangl@itec.uni-klu.ac.at, Telephone: +43 463 2700 3613

H.H.: E-mail: hermann.hellwagner@itec.uni-klu.ac.at, Telephone: +43 463 2700 3612

C.S.: E-mail: cspielvo@itec.uni-klu.ac.at, Telephone: +43 463 2700 3622

H.B.: E-mail: bischof@icg.tu-graz.ac.at, Telephone: +43 316 873 5014

T.S.: E-mail: sztibor@sztaki.hu, Telephone: +36 1 279 6167

algorithms, when metallic objects, e.g., a prosthesis, are present in the region of interest. They are displayed very dark and this leads the algorithm to increase the dose. This outshining effect results in overexposed images and bad contrast. To overcome this limitation, the metallic objects have to be detected and extracted to make a correction of the automatic dose adjustment.

Especially in industrial segmentation applications like quality control or security, the shapes of the objects of interest are well known. That is why model based segmentation methods are mostly used in such application areas.² Because of the huge assortment of metallic parts used in medical applications, e.g., screws, nails, plates, and combinations thereof, it is not possible to use segmentation methods as these require well known models. Common segmentation methods of x-ray images also rely on a special image recording method, so called dual energy.³ Two images of the same ROI are taken, one with low energy and one with high energy. The received images are combined to increase feature information and consequently the segmentation success. The main drawback of this method is that the x-ray tube has to be reloaded with different energies. This reloading process takes too much time and is too slow for real time applications as needed in our case. To overcome these limitation, the use of segmentation methods based on simple efficient algorithms is necessary. Additionally, features which can be extracted with limited complexity need to be investigated.

The remainder of this paper is organized as follows. In Section 2, the characteristic features of metallic occurrence in images are discussed. Section 3 describes our approach for fast metal extraction and Section 4 shows experimental results. Finally, our conclusions are presented in Section 5.

2. FEATURES OF METALLIC OBJECTS IN MEDICAL X-RAY IMAGES

In order to implement a successful segmentation algorithm it is necessary to identify certain characteristic features of an X-ray radiograph. Therefore, we discuss features like grayscale distribution, edges, shape, and texture of metals and their distinction to bone fragments and soft parts which are not objects of interest.

2.1. Grayscale distribution

When we are looking at x-ray radiographs containing metal, the metallic objects occur very dark because they are absorbing a lot of x-rays before they reach the detector. An example is shown in Figure 1(a). To visualize which additional objects own the same gray values, all pixels of the image with values within the grayscale distribution of the metal were highlighted as shown in Figure 1(b). It shows that metallic parts are not the darkest objects in the radiograph, i.e., bones or bone fragments can also appear very dark.

2.2. Edges

Metallic plug-in components like screws, nails or plates are always fixed at bone fragments. So they should cause edges at their borders because distinct changes of gray values appear at the transition to bones. Figure 1(c) shows an edge image of Figure 1(a) which was generated by a smoothing median filtering and a thresholded Sobel operation. It can be seen that the metal produces distinct edges along its boundaries. It also can be noticed that the metal contour is broken at partly smooth transitions to bone fragments. It is also possible that the contour is crossed by other edges caused by transitions from bone fragments to soft parts as shown in Figure 1(c). This would cause problems when using edge based segmentation methods.

2.3. Shape

There are a lot of medical plug-in components with different shapes. Screws, nails, plates etc. can also appear in combination like in Figure 1(a). The plate is fixed with screws on the bone. It is easy to see that the use of model based segmentation methods is impossible in this case. In addition, the images are taken from different positions, so the same objects appear with different shapes at different angles.

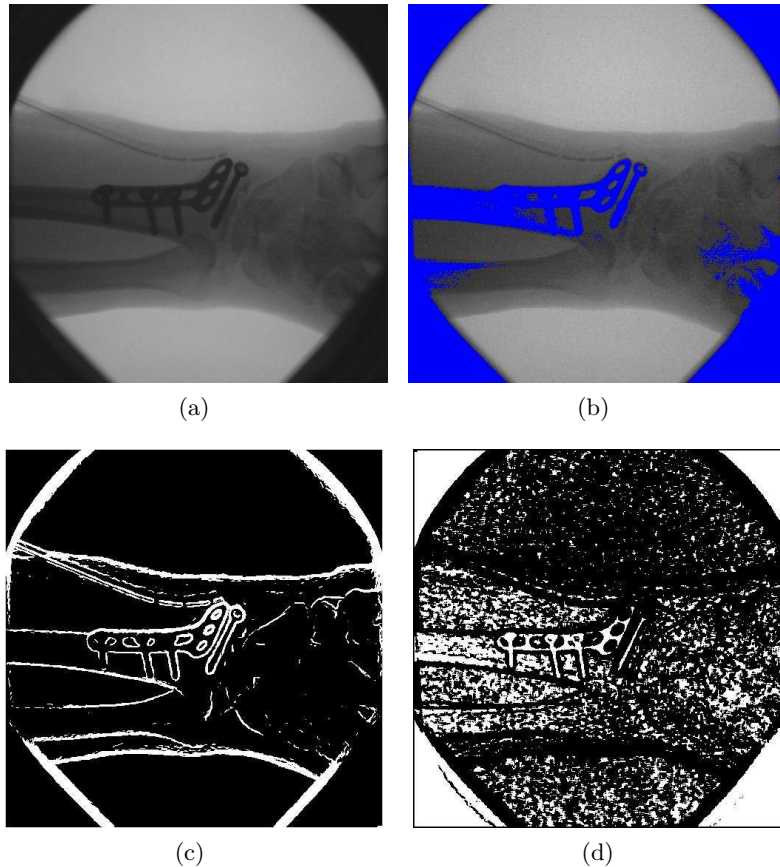


Figure 1. (a) Source image with metallic objects; (b) Highlighted "metal" gray values of (a); (c) Binary edge image of (a); (d) Homogeneity of (a).

2.4. Texture

The surface of metallic components seems to have a smooth texture in the image. Figure 1(d) shows the result of a statistical texture measurement, which was created by a thresholded nonlinear Mean Absolute Deviation (MAD) filtering through a 5x5 mask. The white regions represent homogeneous regions with MAD values less than the selected threshold value. Similar results were obtained by nonlinear variance filtering: metallic objects consist of homogeneous regions but bone segments can also appear as homogeneous as metals do.

The conclusions resulting from the feature examination are as follows. The set of useful features which are the basis to design an automatic extraction process are the grayscale distribution, the distinct edges and the smooth surface of the metallic regions. Because of the wide variation of possible shapes of metallic plug-in components, it is impossible to use known models to make a decision whether a region represents a metal or not. For this reason the shape of a region is not helpful for solving the extraction problem.

3. EXTRACTION OF METALLIC OBJECTS

Our approach to extract metallic objects of medical x-ray images consists of three well known steps in image analysis: preprocessing, segmentation and classification. They all rely on basic, computationally cheap algorithms to limit processing time.

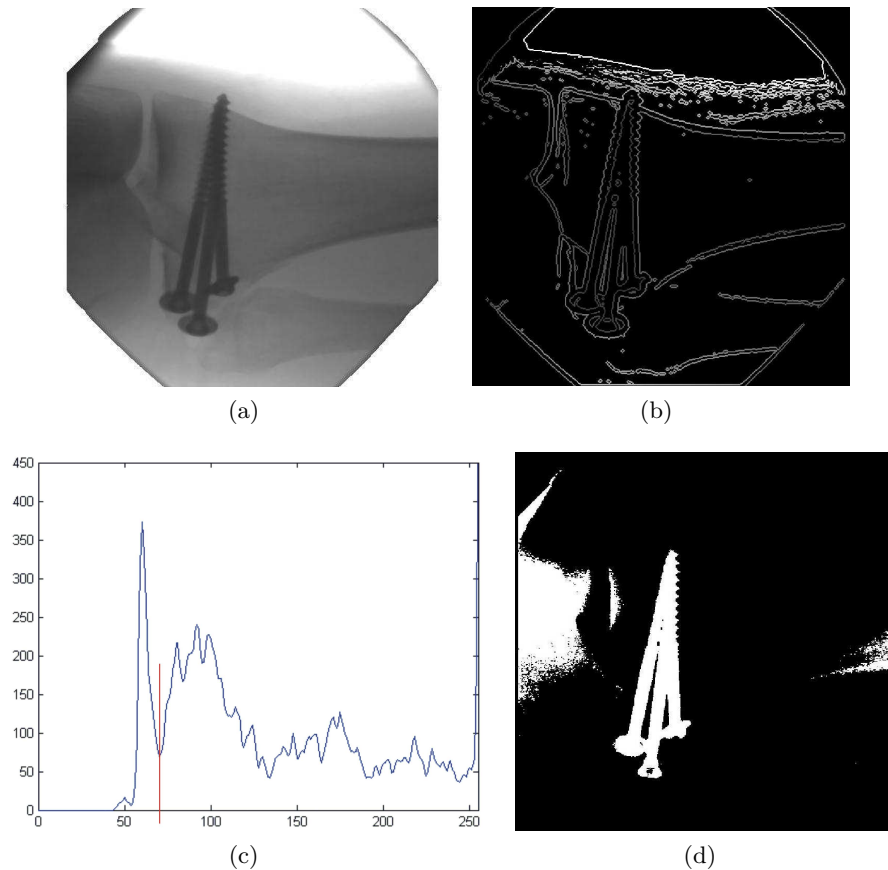


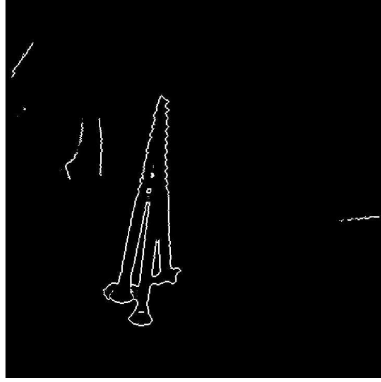
Figure 2. (a) Preprocessed input; (b) Borders of edges; (c) Histogram of (b); (d) Segmentation result.

3.1. Preprocessing

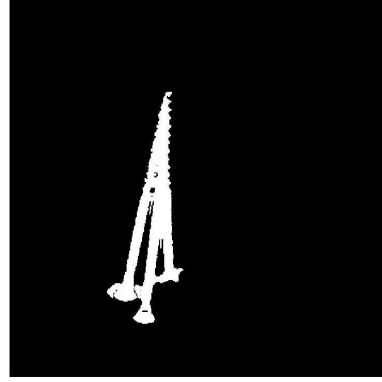
Preprocessing comprises two simple steps. First, a median filter is applied to reduce noise and to be able to get a clean edge image.⁴ Second, the iris is removed by setting pixels to white step by step beginning from the left and right borders until a distinctive changing gray value is detected. This is needed because the iris has the same features as metal, so it has to be excluded from the segmentation process. Figure 2(a) illustrates a result of this step.

3.2. Segmentation

The segmentation process relies on the features of grayscale distribution and the edges of the metallic objects. To separate objects by finding the most appropriate thresholds automatically, the idea is to consider only pixels that are near the metal borders because metals are fixed at bones. This indicates, that at the one side of the border, pixels of metal and at the other side pixels of bones are present. In a local grayscale distribution of only those pixels, a distinct partition should be obtained. Therefore, a binary edge image which results from a simple thresholded absolute addition of horizontal and vertical Sobel operations of the preprocessed input image is needed. To focus on border pixels of the edge image only, an XOR combination of the binary edge image and its dilated version is applied. The conjunction of this result and the original input image is shown in Figure 2(b). The smoothed histogram of this image, which was obtained by a convolution with a Gaussian kernel, is shown in Figure 2(c). It can be seen that there exist distinct local minima. Those minima are selected for optimum threshold values to apply them to the original input image.⁴ Metals occur dark in the image, so the range for threshold selection can be limited at about one third of the total range of gray values. Figure 2(d) shows the result of one threshold applied, which is marked in the histogram (Figure 2(c)). The screws which are our



(a) Conjunction of object borders and edge image



(b) Result after keeping regions with $c_i \geq 70\%$

Figure 3. Classification using correlation of edges

	Resolution	# Metallic Objects.	TP	FP	$D(\%)$	P_{FP}
With metals	high	1419	1208	128	85	0.13
Without metals	high	0	-	19	-	0.10
With metals	low	1419	1054	257	74	0.26
Without metals	low	0	-	48	-	0.24

Table 1. Evaluation of effectiveness and performance based on original (high) and downscaled (low) resolution of input images.

objects of interest are segmented but also some bone fragments are located there. Thus, a further classification process is needed where all non-metallic objects are rejected.

3.3. Classification

The unsupervised classification relies on possible features of metallic objects. First of all, small objects, even if they are representing metals, have no effect in contrast adjustment, so they can get rejected. This is easy and fast because the area of each object can be obtained by the labelling process without much overhead.

Second, metals produce sharp edges (like seen in Section 2.2) in the image. Thus, there is a high degree of correlation between object borders and the edges of a metallic object. The correlation degree c_i for each object i between the borders B_i of an object and the edge image K can be obtained by $c_i = \frac{\sum_1^j AND(B_i, K)}{\sum_1^j B_i}$, where j is the total number of pixels per image. The calculation of K and B can also be done by fast edge detectors like Sobel operators and morphologic operations. Figure 3(a) shows the conjunction of an image of all object borders and the edge image. It can be recognized that the correlation between the borders of metal and its edges is rather high whereas the correlation of other fragments is rather low. The result after rejecting all objects with $c_i < 70\%$ is shown in Figure 3(b). It can be seen that only the region representing the metal remains.

A third optional feature is the homogeneity degree of an object i that can be obtained by $h_i = \frac{M_i}{A_i}$, where M_i is the sum of object pixels with a MAD value lower than a specific low threshold T_h . A_i represents the area of the object i . Regions with low degree of homogeneity can be rejected. However, the nonlinear MAD filtering is more CPU intensive; yet, there are very few objects left for which this calculation has to be done.

4. EXPERIMENTAL RESULTS

We have implemented a prototype for evaluating the effectiveness and performance of this approach using C++ and a special library called the “Intel Integrated Performance Primitives (IPP)”⁵ which provides elementary

	Resolution	$T_{min}(ms)$	$T_{max}(ms)$	$T_{av}(ms)$
With metals	high	27.2	141.9	73.2
Without metals	high	26.8	138.6	71.4
With metals	low	8.7	51.4	24.2
Without metals	low	8.5	49.7	23.5

Table 2. Evaluation of effectiveness and performance based on original (high) and downsampled (low) resolution of input images.

functions for image processing that are optimized for the specific processor in use. The evaluation is based on 1200 different input images where 200 of them contain no metallic regions. The original input images have a resolution of 512x512 pixels with 8 bit gray value depth. In addition, the same evaluation has been performed with a reduced image size of 256x256 pixels. The rescaling was done by discarding every second pixel and row. Although this method is suboptimal, it turned out to be the fastest. A separation of metal containing and non-metal containing inputs was also done like shown in Table 1. The parameters for classification were set to:

- $A_{min} = 160$ pixels (for high resolution)
 $A_{min} = 40$ pixels (for low resolution)
- $c_i > 85\%$
- $h_i > 70\%$, $T_h = 6$

4.1. Effectiveness

To obtain an objective measure of extraction efficacy, true positive (TP) and false positive (FP) objects of interest were counted which are the basis for the statistical evaluation. The degree of detection success D was determined by $D(\%) = \frac{\#TP}{\#metals} \times 100$ and the average probability of falsely detected metallic objects per image P_{FP} was calculated by $P_{FP} = \frac{\#FP}{\#images}$. The detection rate with only a few false positive detections is quite good like shown in Table 1. The reason why a few metallic regions are not detected, is that they could not be separated from bone fragments in the grayscale domain. Such wrongly segmented regions get rejected by the classification step.

With the use of downsampled images the success is decreasing because of loss of image information. Similar effects can be recognized for the number of false positives; they are increasing for the low resolution of the input images.

4.2. Quality

In order to obtain the correlation of successfully extracted metallic objects and the real metallic regions, binary masks of the real metal shapes were created by hand. A set of $n = 100$ different images containing metals were compared this way. The evaluation relies on the sum of remaining binary image pixels of an XOR combination (Figure 4(e), 4(f)) of the binary result R_i (Figure 4(c), 4(d)) and the hand-created binary mask M_i (Figure 4(b)) of a source image i (Figure 4(a)). We defined the average correlation degree E_{av} by $E_{av}(\%) = \frac{\sum_{i=1}^n \left[1 - \frac{\sum XOR(R_i, M_i)}{\sum M_i} \right]}{n} \times 100$. We obtained for the high resolution images $E_{av} = 81\%$ and for the low resolution images $E_{av} = 68\%$. In general, the correlation for low resolution results is lower, especially at the borders of the regions. The reason for this drawback is the information loss caused by the rescaling process.

4.3. Performance

The performance measurements were performed on a system with a 2.4 GHz Intel Pentium IV processor and 1 GB DDR-RAM. The individual processing time depends on the number of applied thresholds and the number of segmented objects needed to be considered in the classification process.

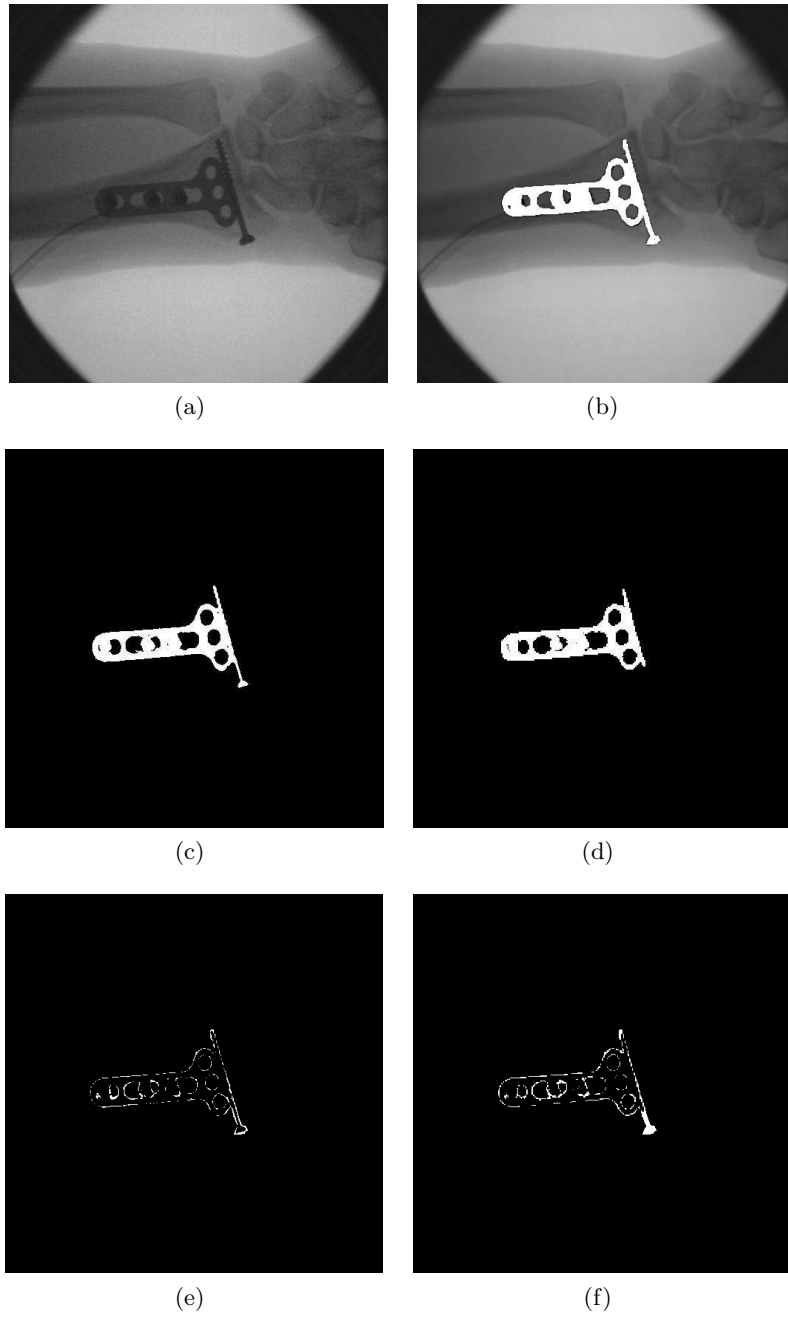


Figure 4. (a) Source image with metallic plate; (b) Mask of metal created by hand; (c) Full resolution extraction result; (d) Half resolution extraction result; (e) XOR combination of (b) and (c); (f) XOR combination of (b) and (d).

Task	$T_{av}(\%)$
Preprocessing	7.6
Segmentation	33.7
Labelling	13.3
Classification	45.4

Table 3. Average relative CPU time of main tasks.

As Table 2 shows, the processing time of images containing metallic regions and those that do not, do not differ significantly. The reason is that every possible object has to be classified, even it is not representing a metal. The algorithm takes about one third of the time for the downscaled images as compared to the original image format (including the downscaling process) but with the drawback of reduced detection efficiency. Table 3 shows the average relative CPU time of the four main tasks of our approach. It can be seen that the classification is the most time consuming part.

5. CONCLUSION

We have presented a fast unsupervised approach for metal extraction to be able to take corrective actions in automatic contrast adjustment of modern x-ray systems. Characteristic features of metallic occurrence in x-ray images were discussed and examined for simple extraction. It is necessary to use fast methods for the whole extraction process. Thus, an efficient way for segmentation and classification was discussed which is based on useful features like grayscale distribution, edges, and homogeneity of metallic occurrence in x-ray images. An evaluation was done which showed good results in detection success, quality, and also in performance. For the use case of contrast adjustment it would cause problems if many false positive metallic regions were detected. Thus, it would be better to use more restrictive classification parameters, even if some true positives got lost. To enhance performance by the use of image series of different angles, it would be possible to limit the search area by predicting locations of metals based on previous detected locations of metallic regions. To improve quality and effectiveness, it would be possible to use a combination of this approach with a region growing algorithm.⁴⁶⁷ But this would be more time intensive and a suitable safe way for seed-pixel selection has to be found in order to avoid additional false positives.

ACKNOWLEDGMENTS

We would like to acknowledge the Siemens Medical Group, Erlangen, Germany for the provided source image data sets and their excellent support.

REFERENCES

1. M. Citak, J. Geerling, D. Kendoff, M. Richter, T. Huefner, and C. Krettek, "Iso-c 3d navigated drilling of osteochondral defects of the talus: A cadaver study," in *Proceedings of the Scientific Workshop on Medical Robotics, Navigation and Visualization*, T. M. Buzug and T. C. Lueth, eds., pp. 118–121, 2004.
2. G. Behiels, D. Vandermeuleb, and P. Suetens, "Statistical shape model-based segmentation of digital x-ray images," in *IEEE Workshop on Mathematical Methods in Biomedical Image Analysis (MMBIA'00)*, June 2000.
3. P. Smyth, C. Taylor, and J. Adams, "Automatic measurement of vertebral shape using active shape models," in *3rd IEEE Workshop on Applications of Computer Vision (WACV'96)*, Dec. 1996.
4. M. Sonka, V. Hlavac, and R. Boyle, *Image Processing: Analysis and Machine Vision*, Brooks/Cole Publishing Company, Pacific Grove, CA, 2nd Edition 1998.
5. *Intel Integrated Performance Primitives*, <http://www.intel.com/software/products/ipp/>, Dec. 2005.
6. R. Pohle and K. Toennies, "Segmentation of medical images using adaptive region growing," in *Proceedings of SPIE Medical Imaging vol. 4322*, pp. 1337–1346, 2001.
7. J. Xuan, T. Adali, and Y. Wang, "Segmentation of magnetic resonance brain image: Integrating region growing and edge detection," in *Proceedings of the 1995 International Conference on Image Processing (ICIP)*, vol. 3, p. 3544, Oct. 1995.